Binding of Oligoarginine to Membrane Lipids and Heparan Sulfate: Structural and Thermodynamic Characterization of a Cell-Penetrating Peptide†

Elisabete Gonçalves,‡ Eric Kitas,§ and Joachim Seelig*,‡

Division of Biophysical Chemistry, Biozentrum, University of Basel, Klingelbergstrasse 70, CH-4056 Basel, Switzerland, and Pharma Division, Preclinical Research, F. Hoffmann-La Roche Limited, CH-4070, Basel, Switzerland

Received September 10, 2004; Revised Manuscript Received November 16, 2004

ABSTRACT: Cell-penetrating peptides (CPPs) comprise a group of arginine-rich oligopeptides that are able to deliver exogenous cargo into cells. A first step in the internalization of CPPs is their binding to the cell surface, a reaction likely to involve membrane phospholipids and/or heparan sulfate proteoglycans (HSPGs). The present work characterizes the interaction of R_9, one of the most efficient CPPs, with either heparan sulfate (HS) or lipid vesicles composed of 1-palmitoyl-2-oleoyl-*sn*-glycero-3-phosphatidylcholine (POPC) and 1-palmitoyl-2-oleoyl-*sn*-glycero-3-phosphatidylglycerol (POPG). Isothermal titration calorimetry shows that R_9 binds to HS with high affinity. Assuming that HS has *n* independent and equivalent binding sites for R_9, we find an association constant of 3.1×10^6 M^{-1} at 28 °C. At this temperature, the reaction enthalpy is $\Delta H^\circ_{pep} = -5.5$ kcal/mol and ∼7 R_9 molecules bind per HS chain, which is equivalent to ∼0.95 cationic/anionic charge ratio. ΔH°_{pep} decreases in magnitude upon an increase in temperature, and the reaction becomes entropy-driven at higher temperatures (≥37 °C). The positive heat-capacity change entailed by this reaction ($\Delta C^\circ_P = +167$ cal mol^{-1} K^{-1}) indicates the loss of polar residues on R_9−HS binding, suggesting that hydrophobic forces play no major role on binding. Calorimetric analysis of the interaction of R_9 with POPC/POPG (75:25) vesicles reveals an association constant of 8.2×10^4 M^{-1} at 28 °C. Using a surface partition equilibrium model to correct for electrostatic effects, we find an intrinsic partition constant of ∼900 M^{-1}, a value that is also confirmed by electrophoretic mobility measurements. This corresponds to an electrostatic contribution of ∼33% to the total free energy of binding. Deuterium nuclear magnetic resonance (NMR) shows no change in the headgroup conformation of POPC and POPG, suggesting that binding takes place at some distance from the plane of the polar groups. ^{31}P NMR indicates that the lipid bilayer remains intact upon R_9 binding. The fact that R_9 binds with greater affinity to HS than to anionic lipid vesicles makes the former molecule a more likely target in binding this CPP to the cell surface.

New therapeutic approaches such as gene- or protein-based therapies rely on the efficient uptake of exogenous macromolecules by living cells. Because of their size and hydrophilicity, most macromolecules of therapeutic interest are unable to cross biological membranes by passive diffusion. As a consequence, the success of such therapies depends, to a great extent, on the development of efficient macromolecular delivery systems.

Cell-penetrating peptides (CPPs),[1] a group of oligopeptides capable of introducing proteins and peptides into cells, are a promising class of molecular transporters (for recent reviews, see refs *1*−*3*). Their transport properties have been demonstrated both *in vitro* and *in vivo* for a variety of hydrophilic macromolecules (*4*−*8*). Two of the best studied CPPs include the peptide derived from the transcriptional activator of the HIV-1 virus, commonly referred to as Tat peptide, and the *Drosophila* Antennapedia homeodomain peptide, known as penetratin. Both peptides represent the transduction domain of the proteins from which they derive (*9*, *10*). The high arginine content of these peptides appears to be related with their membrane translocation properties, because deletion (or replacement by alanine) of a single arginine results in severely reduced internalization (*9*, *11*). This is further supported by the enhanced uptake of arginine homopolymers, whose levels of translocation are increased several fold over those of Tat when the oligoarginine contains 6−12 arginines (*12*, *13*). Medium-length polymers of arginine are also significantly more effective at entering cells than are similar length polymers composed of lysine, ornithine, or histidine (*12*). Modifications in the amino acid side chain (*11*), peptide backbone (*14*), or linearity of the oligoarginines (*15*) do not significantly alter cellular uptake, suggesting that the guanidinium moiety plays a critical role in the translocation process.

Despite the general acceptance of CPPs as macromolecular transporters, their mechanism of internalization remains

† This work was supported by the Swiss National Foundation Grant 31.58800.99.

* To whom correspondence should be addressed. Telephone: +41-61-267-2190. Fax: +41-61-267-2193. E-mail: joachim.seelig@unibas.ch.

‡ Biozentrum, University of Basel.

§ F. Hoffmann-La Roche Limited.

[1] Abbreviations: CPP, Cell-penetrating peptide; R_9, nonaarginine; ITC, isothermal titration calorimetry; MLV, multilamellar vesicle; LUV, large unilamellar vesicle; SUV, small unilamellar vesicle; HS, heparan sulfate; HSPG, heparan sulfate proteoglycan; POPC, 1-palmitoyl-2-oleoyl-*sn*-glycero-3-phosphatidylcholine; POPG, 1-palmitoyl-2-oleoyl-*sn*-glycero-3-phosphatidylglycerol; NMR, nuclear magnetic resonance.

10.1021/bi048046i CCC: $30.25
Published on Web 01/27/2005

poorly understood. Earlier work reports an energy-independent, nonendocytic pathway of cellular uptake, suggesting that these peptides are able to translocate across the cell membrane passively, driven by their concentration gradient (*9*, *10*, *16*). Such observations have, however, been questioned by recent work showing that cell fixation, a typical procedure used in the previous studies, causes relocation of the peptides to the cytoplasm and nucleus and results in apparent cell-membrane translocation (*17*, *18*). Since then, a number of other studies have reexamined the internalization mechanism of CPPs using living cells, demonstrating that endocytosis is definitively one of the pathways of cellular uptake (*19*−*23*). On the other hand, it is also becoming clearer that the internalization mechanism may depend on the chemical nature of the peptide and that some of these CPPs may use more than a single mechanism of internalization. In a study using analogues of several well-known CPPs, Thorén et al. (*24*) show that, while the Tat analogue is taken up by living cells mainly via endocytosis, the oligoarginine analogue appears to use an alternative pathway, because its uptake is observed at 4 °C and in the presence of metabolic inhibitors, two conditions that are known to abolish endocytosis.

The efficient internalization of retroinverso peptides and peptoids shows that the cellular uptake of CPPs is not mediated by a chiral receptor (*11*, *12*, *25*, *26*). When this is combined with the ability of CPPs to translocate into a large variety of cell types, it suggests that an ubiquitous, nonspecific molecular target mediates the binding of these molecules to the cell surface. Heparan sulfate proteoglycans (HSPGs), a group of sulfated polysaccharides anchored to cell-surface polypeptides, are potential receptors for CPPs. Present at the surface of most eukaryotic cells and in the extracellular matrix, these polyanionic molecules mediate the interaction of many pathogens with their host cells (*27*−*29*). They have been implicated in the internalization of several CPPs, including the full Tat protein (*30*, *31*) and the oligoarginine R_9 (*22*), although there is also evidence showing that their presence is not required for the uptake of the Tat peptide (*32*, *33*). Another possible target for CPPs are the lipids found in the cell plasma membrane. Anionic phospholipids have been suggested to form a complex with penetratin leading to its import via the formation of inverted micelles (*26*, *34*). In addition to their potential involvement in binding CPPs to the cell surface, anionic phospholipids may also be involved in the escape of the peptide and its cargo from endosomal compartments. These lipids have been shown to mediate DNA release from cationic lipid−DNA complexes at the endosome level (*35*), thereby avoiding enzymatic degradation of DNA in lysosomes. In a similar manner, they could mediate the release of the CPP cargo before reaching lysosomal compartments and explain the well-documented biological effects of CPPs. In another model, the formation of a transient transmembrane pore-like structure has been proposed for the cell-penetrating peptide Pep-1 (36).

In the present study, we use isothermal titration calorimetry (ITC) to characterize the thermodynamic equilibrium between the oligoarginine R_9, the most efficient CPP presently known, and the two classes of molecular targets mentioned above, namely, heparan sulfate (HS) and membrane phospholipids [1-palmitoyl-2-oleoyl-*sn*-glycero-3-phosphatidylcholine (POPC) and 1-palmitoyl-2-oleoyl-*sn*-glycero-3-phosphatidylglycerol (POPG)]. In both cases, the association reaction is also followed with static light-scattering measurements. In addition, the structure of the lipid bilayer in the presence of R_9 was studied with phosphorus-31 nuclear magnetic resonance (NMR) spectroscopy, combined with deuterium NMR of selectively deuterated lipids.

MATERIALS AND METHODS

Materials. HS, fraction I, sodium salt [from porcine intestinal mucosa, average molecular weight (MW), 14 200 Da; sulfur content, 6.44%] was purchased from Celsus Laboratories (Cincinnati, OH). The oligoarginine R_9 was prepared using standard Fmoc-solid-phase peptide synthesis (*37*). POPC and POPG were obtained from Avanti Polar Lipids Inc. (Alabaster, AL). For solid-state NMR measurements, the lipids were deuterated at the headgroup moiety (i.e., at the α carbon of the choline (POPC) and the glycerol residue (POPG), respectively). All other chemicals were of analytical or reagent grade. Tris buffer (10 or 50 mM tris(hydroxymethyl)aminoethane and 100 mM NaCl at pH 7.4) was prepared from 18 MΩ water obtained from a NANOpure A filtration system.

Preparation of Lipid Vesicles. POPC was dried from a stock solution in chloroform under a gentle stream of nitrogen followed by high vacuum overnight. The amount of POPC was weighed and mixed with a defined volume of a POPG stock solution in chloroform to yield a POPC/POPG molar ratio of 75:25. The solvent was removed in a rotary evaporator, and the thin lipid film was exposed to high vacuum overnight and weighed again. The lipids were resuspended in buffer (50 mM Tris and 100 mM NaCl at pH 7.4) with gentle vortex mixing leading to multilamellar vesicles (MLVs) with a final lipid concentration of 20−30 mM. Small unilamellar vesicles (SUVs) were produced by sonication of the lipid suspension using a titanium-tip ultrasonicator (Branson Sonifier, Danbury, CT) under a nitrogen atmosphere (at 4 °C), until an almost clear solution was obtained (20−30 min). Titanium debris from the sonicator tip was removed by sedimentation in an Eppendorf 5415 C benchtop centrifuge (Vaudaux-Eppendorf AG, Schonenbuch, Switzerland) at 16000*g* for 5 min. Large unilamellar vesicles (LUVs) were prepared by extrusion of MLV suspensions using a hand extruder (Avanti). After five consecutive freeze−thaw cycles, MLVs were extruded 11 times through two stacked polycarbonate membranes with pore diameters of 100 nm (Whatman, Clifton, NJ).

Right-Angle Light Scattering. Static light-scattering measurements were performed in a Jasco FP 777 spectrofluorimeter (Japan-Spectroscopic, Tokyo, Japan). Typically, a 2.8 mL solution of R_9 was titrated with HS or anionic lipid vesicles, at 1 min intervals, under constant stirring. In the HS measurements, a 30 μM R_9 solution was titrated with 5 μL aliquots of 500 μM HS. For the lipid titrations, 10 μL aliquots of POPC/POPG (75:25) sonicated vesicles (26 mM total lipid) were injected into R_9 (8 μM). In both cases, the scattering intensity at 365 nm (with the excitation wavelength set to 350 nm) was measured and recorded as a function of time. The temperature was set to the values indicated in the captions of the figures.

ITC. All measurements were made with a MicroCal VP-ITC calorimeter (MicroCal, Northampton, MA). To avoid

air bubbles, all solutions were degassed under vacuum prior to use. Lipid titrations were performed by injecting 10 μL aliquots of POPC/POPG (75:25) sonicated vesicles (18.2 mM total lipid) into the calorimeter cell (V_{cell} = 1.4037 mL) containing R_9 (40−60 μM), at constant time intervals of 5 min. For the HS titrations, the R_9 concentration in the calorimeter cell was typically 95 μM and 5 μL aliquots of 200 μM HS were injected every 6 min. To minimize the error associated with diffusion from the syringe during baseline equilibration, the first injection was set to 2.5 μL and the associated heat was not included in the data analysis. A control titration, in which lipid vesicles or HS were titrated into pure buffer, was used to correct for the heat of dilution. Raw data were processed using Origin graphing software provided with the instrument. The temperature was set as indicated in the captions of the figures. At all temperatures, the binding of R_9 to lipids and HS is reflected in a strong exothermic reaction. Near the end point of the titration (approximate charge neutralization of R_9), an additional small endothermic peak is observed, which is less than 10% of the exothermic reaction. At low temperatures or high salt concentrations (≥200 mM NaCl), no such effect is seen. We attribute this additional reaction to the formation of larger aggregates (*38*).

NMR Spectroscopy. All spectra were acquired at a magnetic field strength of 9.4 T. For the ^{2}H NMR measurements, a quadrupole echo sequence was employed using a recycle delay of 250 ms. ^{31}P NMR spectra were recorded using a Hahn echo sequence with broadband proton decoupling (WALTZ-16) and a recycle delay of 6 s. The chemical-shielding anisotropy, $\Delta\sigma$, was measured as full width at 10% maximum intensity. Multilamellar lipid samples were prepared using typically 25 mg of total lipids and 100−150 μL of deuterium-depleted water. The peptide was added before vortexing the lipid film.

Electrophoretic Mobility. The electrophoretic mobility, *u*, of POPC/POPG (75:25) MLVs was measured in a Rank Brothers Mark II instrument (Bottisham, Cambridge, U.K.), in the presence of various concentrations of R_9. The lipid vesicles (1.25 mM total lipid) were inserted into the cylindrical cell (V_{cell} = 4 mL), and 10 μL aliquots of a R_9 solution (188.8 μM) were added at regular time intervals. The ζ potential was calculated from *u* using the Helmholtz−Smoluchowski equation (*39*). Samples were prepared in Tris buffer (10 mM Tris and 100 mM NaCl at pH 7.4), and all measurements were done at room temperature (23 °C).

RESULTS

Binding of R_9 to Anionic Lipid Vesicles: Calorimetric Studies. The interaction of R_9 with anionic lipid vesicles was studied by ITC. After the usual protocol for lipid-into-peptide titrations (*40*), a diluted solution of R_9 (60 μM) was filled into the calorimeter cell (V_{cell} = 1.4037 mL) and small aliquots (10 μL) of a concentrated vesicle suspension (18.2 mM total lipid) were injected at regular time intervals (5 min). Figure 1A shows a representative calorimetric trace obtained at 28 °C by titration of R_9 with POPC/POPG (75:25) sonicated vesicles. The corresponding titration curve is shown in Figure 1B, where the reaction heats are plotted as a function of the lipid/peptide molar ratios. The heats of reaction were obtained by integration of the titration peaks

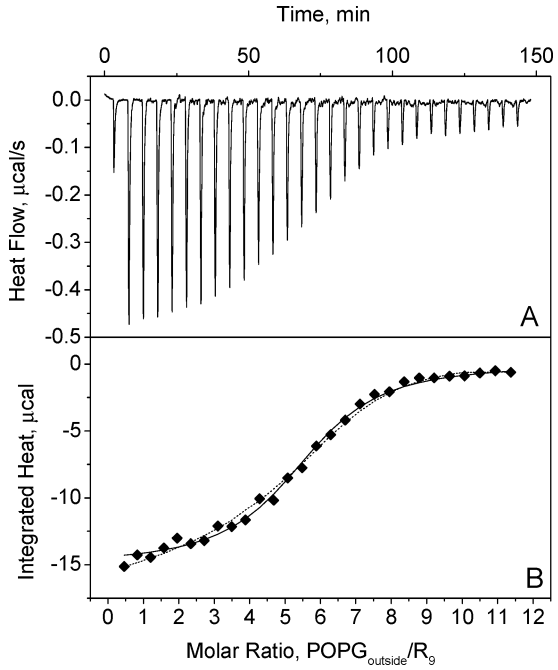

FIGURE 1: Titration of anionic lipid vesicles into R_9. (A) Calorimetric trace obtained at 28 °C by titration of POPC/POPG (75:25) sonicated vesicles (18.2 mM total lipid) into a solution of R_9 (60 μM). Each peak corresponds to the injection (at 5 min intervals) of 10 μL of lipid vesicles into the calorimeter cell (V_{cell} = 1.4037 mL), except for the first peak where only 2.5 μL was injected. (B) Heats of reaction (integrated from the calorimetric trace) plotted as a function of the POPG/R_9 molar ratio. Only the POPG in the outer monolayer of the lipid vesicles (67% = 3.08 mM) is considered to be available for binding. The solid line is the best fit to the experimental data (◆) using the complex formation model, and the dashed line corresponds to the surface partition equilibrium model (cf. Table 1 for parameters). Buffer, 50 mM Tris and 100 mM NaCl at pH 7.4.

shown in Figure 1A and are corrected for the heats of dilution of the lipid vesicles (∼ −1.3 μcal) obtained in a separate lipid-into-buffer titration (not shown).

The sigmoidal shape of the titration curve lends itself to a simple interpretation (*40*, *41*). Initially, a large excess of free R_9 is present in the calorimeter cell, and most of the injected lipid binds to the peptide. As a consequence, a relatively constant heat of binding (∼ −15 μcal) is observed in the first few injections, which, when normalized per mole of bound lipid, is equal to the lipid molar binding enthalpy, ΔH°_{lip}. In the present case, only the POPG at the surface of the sonicated vesicles is assumed to bind to R_9 (*vide infra*) and a $\Delta H^\circ_{lip} \cong -0.45$ kcal/mol is found. As the titration proceeds, the free R_9 concentration decreases and the binding heats decrease in parallel. At the inflection point of the titration curve, approximately half of the total lipid and peptide are in the bound state, and the ratio of the added POPG (outside) to total peptide is therefore a good estimate of the binding stoichiometry. In Figure 1B, the inflection point occurs at a POPG$_{ouside}$/R_9 molar ratio of $n \cong 5.5$. Finally, saturation of R_9 is eventually achieved, and further injections entail no more heat events besides the heat of dilution of the lipid vesicles. Under such conditions, the peptide molar-binding enthalpy, ΔH°_{pep}, is easily determined from the total heat released in the titration and the amount of peptide in the calorimeter cell. A $\Delta H^\circ_{pep} \cong -2.4$ kcal/mol is determined from Figure 1B. As expected, a

Table 1: Thermodynamic Parameters for R_9 Binding to POPC/POPG (75:25) Sonicated Vesicles at 28 °C[a]

Complex Formation Model				
binding stoichiometry (n)	K (M^{-1})	ΔH°_{pep} (kcal/mol)	ΔG°_{pep} (kcal/mol)	$T\Delta S^\circ_{pep}$ (kcal/mol)
4.9 ± 0.7	$(8.2 \pm 0.6) \times 10^4$	-2.5 ± 0.3	-6.8 ± 0.1	4.3 ± 0.3
Surface Partition Equilibrium Model				
peptide charge (z_P)	K_P (M^{-1})	ΔH°_{pep} (kcal/mol)	ΔG°_{pep} (kcal/mol)	$T\Delta S^\circ_{pep}$ (kcal/mol)
3.9 ± 0.6	900 ± 82	-2.3 ± 0.3	-6.5 ± 0.1	4.2 ± 0.3

[a] Data represent the average ± standard deviation of 3−5 measurements. Buffer, 50 mM Tris and 100 mM NaCl at pH 7.4.

similar value is obtained when ΔH°_{lip} is multiplied by the binding stoichiometry ($\Delta H^\circ_{pep} = n\Delta H^\circ_{lip} \cong -2.5$ kcal/mol).

Analysis of the Titration Curve with Specific Binding Models. While simple and straightforward, the previous analysis does not provide a full thermodynamic characterization of the binding event. For that reason, the data have to be treated with appropriate binding models. The first model considered here is a *complex formation model*, in which each POPG molecule acts as a ligand (L) and the peptide R_9 is assumed to have n equivalent and independent binding sites. This can be described according to (*42*−*44*)

$$\frac{[L]_b}{[P]_t} = \frac{nK[L]}{1 + K[L]} \quad (1)$$

In eq 1, [L] and $[L]_b$ are the concentrations of free and bound POPG lipid, respectively, $[P]_t$ is the total concentration of R_9, and K is the microscopic binding constant. Because of the lack of evidence showing translocation of R_9 across the lipid membrane (*vide infra*), only the POPG in the outer leaflet of the lipid bilayer is considered to be available for binding. On the basis of simple geometric considerations, this is assumed to represent 67% of the total POPG present in sonicated vesicles (*45*). Because of mass conservation, $[L]_b = [L]_t - [L]$ can be expressed as a function of the total (accessible) POPG, $[L]_t$, and the total R_9 concentrations, $[P]_t$ (*38*), which, in turn, may be linked to the calorimetric data using the following equation:

$$\delta Q_i = \Delta H^\circ_{lip}\, \delta[L]_{b,i} V = (\{\Delta H^\circ_{pep}\}/\{n\})\, \delta[L]_{b,i} V \quad (2)$$

where δQ_i is the heat released in injection i, $\delta[L]_{b,i}$ is the change (increase) in the bound POPG concentration upon injection i, and V is the volume of the calorimeter cell (*46*). The solid line in Figure 1B is the best least-squares fit to the data using eqs 1 and 2 and the following set of parameters: $n = 5.5$, $K = 7.5 \times 10^4$ M^{-1}, and $\Delta H^\circ_{pep} = -2.6$ kcal/mol. A summary of the thermodynamic parameters found with this binding model is presented in Table 1.

Despite the good agreement between the experiment and theory, the complex formation model does not take into consideration the electrostatic effects sensed at the membrane surface. To account for such effects, we have treated the data with an alternative binding model, the *surface partition equilibrium model*. Used to describe the binding of a variety of other charged molecules to lipid membranes (*47*−*51*), this model assumes that the peptide (P) *partitions* into the lipid membrane (M) according to

$$\frac{[P]_b}{[M]_t} = K_P [P]_s \quad (3)$$

where $[P]_b$ is the concentration of bound R_9, $[M]_t$ is the concentration of total accessible membrane lipid (POPC and POPG), $[P]_s$ is the concentration of free R_9 at the *surface* of the membrane, and K_P is the chemical partition coefficient. This model has the advantage that, by replacing the R_9 bulk concentration, [P], by its interfacial concentration, $[P]_s$, it accounts for the enhanced R_9 surface concentration induced by the negative electrostatic potential of the lipid membrane. Using the Gouy−Chapman theory of the electrical double layer (for reviews, see ref *52*), it is possible to calculate $[P]_s$ for each point of the titration curve and to determine the partition constant, K_P, and the effective charge of R_9 sensed at the membrane surface, z_P. Our calculations also include Na^+ binding and pH changes at the membrane surface (*53*). The dashed line in Figure 1B is the best theoretical fit to the experimental data with $\Delta H^\circ_{pep} = -2.3$ kcal/mol, $K_P = 900$ M^{-1}, and $z_P = +3.9$. The free energy of peptide binding, ΔG°_{pep}, can be calculated from the partition coefficient K_P according to $\Delta G^\circ_{pep} = -RT \ln 55.5 K_P$, where the factor 55.5 represents the molar concentration of water and corrects for the cratic contribution to the binding event (*42*). The thermodynamic analysis is summarized in Table 1. Two conclusions may be taken from Table 1: (i) the effective charge of R_9 is *lower* than the theoretical value of +9; this is in parallel to the binding stoichiometry given by the complex formation model, which indicates an average of 4.9 ± 0.7 POPG molecules bound per R_9, whereas the effective electric charge of R_9 at the membrane surface found with the surface partition equilibrium model is $z_P = +3.9 \pm 0.6$; and (ii) the partition constant, K_P, in the electrostatic attraction/chemical partition model is approximately 2 orders of magnitude smaller than the microscopic binding constant, K, in the complex formation model. Because electrostatic effects were taken into account in the determination of K_P, this indicates that *electrostatics* play a major role in the interaction between R_9 and POPC/POPG (75:25) vesicles.

Electrophoretic Mobility Studies. The ζ potential, defined as the electrostatic potential at the hydrodynamic plane of shear (2 Å from the membrane surface), can be calculated from the measured values of electrophoretic mobility, u, by the Helmholtz−Smoluchowski equation (*39*). Because ζ is related to the surface charge density of the lipid membrane, it decreases when R_9 binds to the membrane and neutralizes the anionic lipid charges. Such decline in ζ may be predicted using the Gouy−Chapman theory and the surface partition equilibrium model presented above (*54*). We measured the ζ potential of POPC/POPG (75:25) MLVs in the presence of various amounts of R_9, and we obtain a good agreement between the experimental results and the theoretical prediction using the parameters derived from the calorimetric studies (results not shown).

Static Light-Scattering Studies. A turbid solution is obtained when sonicated POPC/POPG (75:25) vesicles are mixed with R_9. Upon addition of the peptide, the lipid vesicles aggregate and/or fuse and the increase in turbidity may be used to follow the association reaction. Figure 2

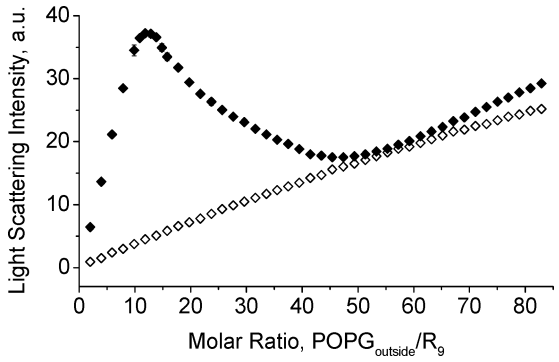

FIGURE 2: Right-angle static light scattering obtained by titration of lipid vesicles into R_9. Each data point corresponds to the injection of 10 μL of POPC/POPG (75:25) sonicated vesicles (26 mM total lipid) into a solution of R_9 (8 μM). Only the POPG in the outer monolayer of the lipid vesicles (67% = 4.4 mM) is assumed to be available for binding. The open symbols represent a control titration where the same suspension of sonicated vesicles is injected into pure buffer (10 mM Tris and 100 mM NaCl at pH 7.4). The injections were done at 1 min intervals, at room temperature, under constant stirring.

shows scattering intensity data when small aliquots of lipid vesicles (26 mM total lipid) are titrated into a 8 μM R_9 solution (◆) or into pure buffer (◇). As in the studies described above, the POPG/R_9 molar ratios were calculated assuming that only the POPG at the outside of the vesicles binds to the peptide. The scattering intensity of the R_9 solution increases almost linearly upon addition of sonicated vesicles, reaching a maximum value at a POPG$_{outside}$/R_9 molar ratio of 12.3 ± 0.7. Interestingly, a decrease in scattering is observed beyond this point, indicating that some of the larger aggregates/complexes are brought back into solution upon addition of more lipid. The residual scattering intensity can be attributed to the intrinsic scattering of the lipid vesicles, because a similar increase is observed when sonicated vesicles are titrated into pure buffer (◇).

The maximum light scattering occurs at a POPG$_{outside}$/R_9 molar ratio, which is more than twice as large as the stoichiometry derived from the complex formation model with $n = 5.5$. As mentioned above, R_9 carries 9 positive charges and only about 60% of those are electrically neutralized with $n = 5.5$. A full neutralization on the *same* phospholipid vesicle may not be possible for steric reasons, because the guanidinium side groups of an extended chain alternate in opposite directions. However, intervesicle bridges may be formed at sufficiently high lipid concentrations, explaining the scattering maximum at POPG$_{outside}$/R_9 = 12.3.

Deuterium and Phosphorus-31 NMR Studies. Solid-state NMR was used to get further structural information about the interaction between R_9 and anionic lipid membranes (Figure 3). NMR spectra were obtained with POPC/POPG (65:35) suspensions mixed with R_9 at a POPG/R_9 ratio of 6:1, which is close to the stoichiometric parameters deduced above. The phosphorus-31 NMR spectra shown in Figure 3A is typical for a lipid bilayer with a separation of $\Delta\sigma = -47.5$ ppm between the low- and high-field edges. This chemical-shielding anisotropy is not different from that of a POPC/POPG (65:35) bilayer in the absence of R_9 with $\Delta\sigma = -45$ ppm at 25 °C (*55*). Despite the strong electrostatic interaction between R_9 and POPG, it is still possible to resolve two separate resonances for POPG and POPC at the 90° edge of the spectrum.

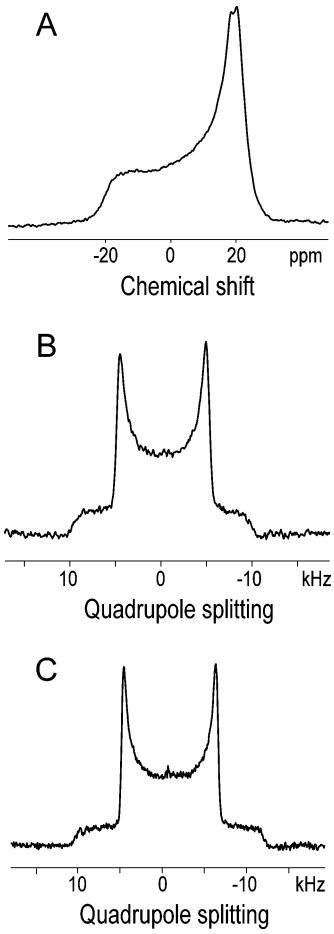

FIGURE 3: Solid-state NMR spectra of multilamellar POPC/POPG (65:35) dispersions in the presence of R_9. The POPG/R_9 molar ratio is 6:1 in all spectra. (A) ^{31}P NMR spectrum. (B) ^{2}H NMR spectrum where POPC is selectively deuterated at the α segment of the choline moiety ($POCD_2CH_2N(CH_3)_3$), while POPG remains protonated. (C) ^{2}H NMR spectrum where POPG is selectively deuterated at the α segment of the glycerol headgroup ($POCD_2$-$CHOHCH_2OH$), while POPC remains protonated (see the text for numerical values of quadrupole splittings and chemical-shielding anisotropies). The exact composition of sample B was 16.91 μmol of POPC, 10.24 μmol of POPG, 1.7 μmol of R_9 and 100 μL of deuterium-depleted H_2O, leading to a POPG/R_9 molar ratio of 6.02. The NMR samples were prepared without salt, and electrostatic attraction is high. Under these conditions, virtually all of the peptide is bound to the membrane surface and the extent of binding $X_b = n_R^b/n_L^o$ is 0.55 if n_R^b denotes the total number of bound arginine residues and n_L^o denotes the total number of lipid molecules.

The lipid−peptide interaction was further studied with deuterium NMR and headgroup deuterated lipids. α-CD_2-POPC ($POCD_2CH_2N(CH_3)_3$) or α-CD_2POPG ($POCD_2$-$CHOHCH_2OH$) were mixed at the above-mentioned ratio with their nondeuterated counterpart. The deuterium NMR spectra of the multilamellar liposomes in the presence of R_9 (POPG/R_9 ≅ 6) are shown for membranes with α-CD_2POPC/POPG (POPC/α-CD_2POPG) in Figure 3B (and Figure 3C). The quadrupole splittings, i.e., the separations between the most intense peaks in the powder-type spectra, are $|\Delta\nu_\alpha| = 9.4$ and 10.7 kHz for α-CD_2POPC and α-CD_2POPG, respectively. Surprisingly, these values are virtually identical to those observed in control experiments in the absence of peptide (*56*). The deuterium spectra thus support the above

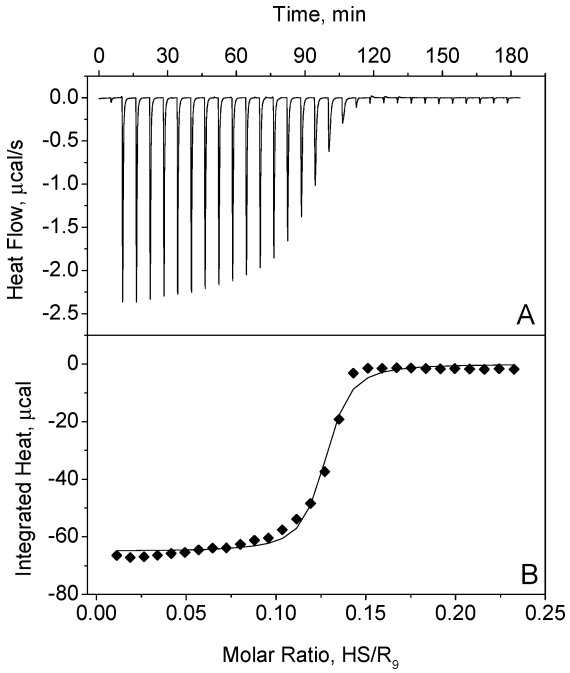

FIGURE 4: Titration of HS into R_9. (A) Calorimetric trace obtained at 5 °C by titration of HS (200 μM) into R_9 (95 μM). Each peak corresponds to the injection (every 6 min) of 5 μL of HS into the calorimeter cell (V_{cell} = 1.4037 mL), except for the first peak, where only 2.5 μL was injected (see the text). (B) Heats of reaction (integrated from the calorimetric trace) plotted as a function of the HS/R_9 molar ratio. The solid line is the best fit to the experimental data (◆) using the binding model described by eq 1 with the parameters listed in Table 2. Buffer, 10 mM Tris and 100 mM NaCl at pH 7.4.

conclusion that the lipids remain organized in a bilayer structure.

It should also be realized that the deuterium NMR spectra are much more sensitive to conformational changes than phosphorus-31 NMR. Because exactly the same quadrupole splittings are recorded with and without R_9, it can be concluded that no conformational changes occur in the POPC and POPG headgroups upon binding of R_9. As detailed in the caption to Figure 3, the ratio of bound arginine residues to total lipid molecules is about 0.55; i.e., each second lipid headgroup should see a cationic arginine. For a large variety of cationic molecules, including amphipathic peptides, quite dramatic changes in the quadrupole splittings of the choline headgroup were observed, even at much smaller binding ratios. For example, the adsorption of the monovalent cationic local anesthetic dibucaine to a POPC membrane changes the quadrupole splitting linearly from +6 to −3 kHz as the extent of binding increases from 0 to $X_b \approx 0.3$ (*57*). The strong binding of R_9 to the lipid membrane without eliciting a corresponding response of the choline dipole is not caused by a lack of sensitivity in the measurement but reveals a new type of binding mechanism (cf. below).

Binding of R_9 to HS: Calorimetric Studies. ITC was further used to study the interaction between R_9 and HS. Figure 4 shows a representative calorimetric trace (Figure 4A) and the corresponding titration curve (Figure 4B) obtained at 5 °C by titration of R_9 (95 μM) with 5 μL aliquots of HS (200 μM). The integrated heats shown in Figure 4B represent the net heats of each injection obtained after subtracting the heats of HS injected into pure buffer. As in the lipid-into-R_9 titration, nearly constant heats are observed at the beginning of the titration (~ -70 μcal). They indicate an almost complete binding of the injected HS caused by the large excess of free R_9 in the calorimeter cell. The molar heat of reaction is $\Delta H^\circ_{HS} = -70$ kcal/mol. On the other hand, at the end of the titration, virtually all R_9 is in the bound state, because the heats measured for the last injections are very small and reflect the heat of dilution of HS. Under these conditions, $\Delta H^\circ_{pep} \cong -9.0$ kcal/mol is determined by dividing the total heat released in the titration (~ -1200 μcal) by the total amount of peptide in the calorimeter cell (133.4 nmol). The ratio $\Delta H^\circ_{HS}/\Delta H^\circ_{pep} = 7.8$ yields the number of R_9 peptides bound to 1 HS molecule.

A long polymer such as HS may be described as a macromolecule with *n* independent and equivalent binding sites for a ligand like R_9. Referred to as the *complex formation model* in the previous section, this model is again described mathematically by eq 1, where, in the present case, L represents R_9 and P represents the HS polymer chain. A full thermodynamic analysis of the HS−R_9 binding equilibrium was done using this binding model. The solid line shown in Figure 4B is the best least-squares fit to the experimental data (◆) using eqs 1 and 2 with the following set of thermodynamic parameters: $n = 7.0$, $K = 3.8 \times 10^6$ M^{-1}, and $\Delta H^\circ_{pep} = -10.3$ kcal/mol. As in the previous studies, the binding stoichiometry, *n*, is defined as the number of ligand molecules bound per macromolecule; it is approximately equal to the inverse of the HS/R_9 molar ratio found at the midpoint of the titration curve ($\sim$0.15 in Figure 4B). The thermodynamic parameters obtained with this binding model are summarized in Table 2.

The influence of temperature on the HS−R_9 interaction was also investigated (cf. Table 2). The enthalpy of binding, ΔH°_{pep}, is exothermic at all temperatures investigated, but it decreases in magnitude with increasing temperature as demonstrated in Figure 5A. As a consequence, while driven by enthalpy at low temperatures ($\leq$28 °C), the reaction becomes entropy-driven at higher temperatures ($\geq$37 °C); this is confirmed by the observed increase in entropy with temperature (Table 2). The slope of the straight line shown in Figure 5A describes the heat capacity change, ΔC°_p, of the HS−R_9 interaction, which is equal to +167 cal mol^{-1} K^{-1} (with respect to R_9). As expected for a charge neutralization reaction, ΔC°_p is *large* and *positive* (*58*, *59*). Inspection of Table 2 further reveals that the binding constant decreases with temperature, as a consequence of the exothermic character of the HS−R_9 interaction. The solid line in Figure 5B describes the predicted temperature dependence of the microscopic binding constant, *K*, based on the van't Hoff relation d ln *K*/d $T = \Delta H^\circ_{pep}/RT^2$ and taking into account the temperature dependence of ΔH°_{pep} (Figure 5A). Within the accuracy of the measurements, a good agreement between experimental data and theory is obtained.

Smooth titration curves as shown in Figure 4 are obtained at low temperatures or at high salt concentrations (e.g., 15 °C and 250 mM NaCl). Under some conditions, a small endothermic reaction was found to be superimposed, starting at the end of the exothermic complex formation. It can be attributed to an aggregation of the R_9−HS complex, presumably caused by cross linking of HS molecules via R_9 bridges. Aggregation is reflected by a turbidity increase in static light scattering (data not shown) and has been observed before

Table 2: Thermodynamic Parameters for R_9 Binding to HS[a]

temperature (°C)	binding stoichiometry (n)	K (M^{-1})	ΔH°_{pep} (kcal/mol)	ΔG°_{pep} (kcal/mol)	$T\Delta S^\circ_{pep}$ (kcal/mol)
5	7.4 ± 0.8	$(4.1 \pm 0.8) \times 10^6$	-9.5 ± 1.3	-8.4 ± 0.1	-1.1 ± 1.3
15	7.9 ± 0.5	$(3.1 \pm 0.2) \times 10^6$	-6.7 ± 0.4	-8.6 ± 0.1	1.8 ± 0.3
28	6.9 ± 0.8	$(3.1 \pm 0.8) \times 10^6$	-5.5 ± 1.2	-8.9 ± 0.2	3.4 ± 0.1
37	10.2 ± 0.9	$(1.3 \pm 0.2) \times 10^6$	-3.0 ± 0.3	-8.7 ± 0.1	5.7 ± 0.3
45	8.7 ± 0.8	$(1.8 \pm 0.1) \times 10^6$	-2.9 ± 0.3	-9.1 ± 0.1	6.2 ± 0.3

[a] Data represent the average ± standard deviation of 3−5 measurements. Buffer, 10 mM Tris and 100 mM NaCl at pH 7.4.

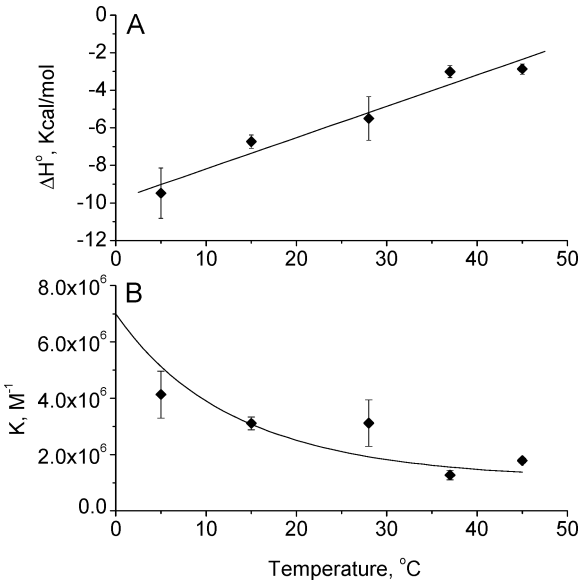

FIGURE 5: Temperature dependence of (A) the reaction enthalpy, ΔH°_{pep}, and (B) the binding constant, K, for R_9 binding to HS. Linear regression analysis of the experimental data in A yields ΔH°_{pep} (kcal/mol) $= -9.854 + 0.167T$ (°C) (—). The solid line in B is the predicted temperature dependence of K using the above regression formula for $\Delta H^\circ_{pep}(T)$.

for the reaction of the TAT protein transduction domain with HS (*38*). Titration isotherms, which displayed an endothermic contribution were therefore evaluated up to the midpoint of the exothermic complex formation. This was possible because of the large binding constant, producing a sharp titration midpoint.

DISCUSSION

The present work characterizes the interaction of R_9 with HS and lipid vesicles at the thermodynamic and mechanistic level. The bilayer membrane is composed of POPC and POPG, two phospholipids commonly found in biological membranes. Both HS and POPG are potential cell-surface targets for the cationic R_9, and investigating the underlying binding equilibrium is relevant for an overall understanding of the internalization mechanism of CPPs.

Thermodynamics of R_9 Binding to HS. In comparing arginine-rich CPPs with their lysine-rich analogues, it was concluded that "arginine thus appears crucial for the cell-surface binding and internalization of CPPs, and there exists a specific interaction between the guanidinium group of arginine and a hydrogen-bond acceptor moiety in the plasma membrane" (*24*). This is supported by the rather extensive literature, which exists on the interaction of polycationic peptides with different types of glycosaminoglycans (*60*−*63*). However, the available quantitative data are mainly concerned with the interaction with heparin, whereas for HS, only a few reports exist (*38*, *64*). This is surprising because heparin is located mainly in the cell interior, whereas HSPGs are ubiquitously distributed across the outer surface of cell membranes. The two species will exhibit different binding properties because HS has a lower extent of sulfation than heparin (heparin ∼ 2.7 sulfate groups per disaccharide, and HS ∼ 1.0 sulfate per disaccharide) (*65*).

The calorimetric data presented here shows that R_9 has a strong affinity for HS. A binding constant of 3.1×10^6 M^{-1} is found at 28 °C (Table 2), which is equivalent to a dissociation constant of 0.3 μM. Although this value is slightly higher than the $K_d = 0.1$ μM measured by affinity chromatography for the R_9−heparin binding equilibrium (*22*), this difference can be explained by the lower extent of sulfation of HS when compared to heparin (*65*).

As anticipated from the structure of the reacting molecules, *electrostatics* is a major component of the R_9−HS interaction. Binding stoichiometries close to charge neutrality are obtained when the molar R_9/HS ratios are converted to charge ratios. Relying on the sulfur content (6.44%) provided by the manufacturer to estimate the number of sulfates and considering that one carboxylate group is present per HS disaccharide (*65*), we estimate an average of ∼60 anionic charges per HS molecule. As a consequence, the molar R_9/HS ratios of 5 and 7 found in the static light scattering (data not shown) and calorimetric studies (Table 2) correspond to electric charge ratios of 0.75 and 1.05, respectively, values that are very close to charge neutralization. Also supporting the involvement of electrostatics in the association reaction is the large and positive change in heat capacity of this reaction ($\Delta C^\circ_p = +167$ cal mol^{-1} K^{-1}) (*58*, *59*).

The HS employed in this study has a MW of 14.2 ± 2 kDa, corresponding to about 30.6 ± 4.3 disaccharide units (MW ∼ 464). Because each HS molecule binds 7−8 R_9 peptides, the arginine/disaccharide ratio is in the rage of 1.9−2.7. If each disaccharide unit carries 1 sulfate and 1 carboxyl, an arginine/HS ratio of 2 would lead exactly to charge neutralization. A ratio of 2 has been found in early circular dichroism (CD) studies for the polylysine−HS system (*62*). However, for the polyarginine−HS system, the same study reports a ratio of ∼1 only. The authors indicate that the evaluation of the CD spectra was difficult because of turbid solutions.

Electrostatics is not the only force providing stability to the R_9−HS complexes. Considering the well-known ability of the guanidinium group to form hydrogen bonds with sulfate and carboxylate groups (*66*), it is very likely that *hydrogen bonding* is the second major type of interaction taking place in the R_9−HS binding equilibrium. This would explain the favorable ΔH°_{pep} found at all temperatures (Table 2), a fact that is not commonly observed in purely electrostatic interactions involving polyelectrolytes. As a

result of an increase in entropy because of counterion release, these are usually accompanied by small and, in many instances, unfavorable binding enthalpies (*67*). We are presently studying the salt dependence of the R_9−HS association constant to discriminate the electrostatic from the nonelectrostatic component of this reaction.

In a related study, synthetic peptides having the general sequence R_nW were titrated with heparin (MW 4800) (*64*). For R_9W, a binding constant of 7.6×10^6 M^{-1} was found, rather similar to the results observed for the binding of R_9 to HS. As the number of arginines decreased, the binding affinity remained fairly constant until $n = 4$. In parallel, the maximum number of ligands, q, per heparin increased, and the product of the two numbers remained also constant. Independent of the length of the polycation R_nW, the same number of arginine residues was always bound at the saturation limit. While R_9 is an excellent CPP, shorter R_n such as R_4 or R_5 are not. Because the binding affinities of these molecules to heparin are very similar, the differences in their transport affinity cannot be explained by simple thermodynamic arguments. Using confocal microscopy, we have shown for mouse fibroblasts that the transport of the TAT protein transduction domain across the biological membrane is coupled with an aggregation phenomenon or patch formation at the membrane surface and that HS is necessary for this process (*68*).

Even though not the primary purpose of this work, we may speculate that R_9 has the right length to link together a sufficient number of HS-carrying membrane proteins. This may induce aggregate formation on the surface of the living cell, followed by a still unknown translocation mechanism. Shorter arginine chains do not seem to have this capability, but this has yet to be tested under *in vivo* conditions. We are presently studying the effect of R_9 on *in vivo* cell cultures.

A purely physical−chemical mechanism has been proposed for the transport of R_8 across the lipid membrane (*69*). In these experiments, the polarity of the arginine residues was attenuated by ion-pair complex formation. In addition, an electric gradient was postulated to drive the complex across the membrane.

Thermodynamic and Structural Aspects of R_9 Binding to Anionic Lipid Vesicles. The characteristic sigmoidal shape of the calorimetric titration curve (Figure 1) and the increase in scattering intensity observed when R_9 is mixed with POPC/POPG (75:25) vesicles (Figure 2) are unequivocal evidence that R_9 binds to anionic lipid vesicles. Treating the calorimetric data with the complex formation model used in the analysis of the R_9−HS equilibrium, we find an association constant of 8.2×10^4 M^{-1} at 28 °C (Table 1). This value is 2 orders of magnitude smaller than that found for the R_9−HS interaction (Table 2), and binding to HS is thus strongly favored if both HS and POPG should be present at the cell surface. A similar conclusion has been made for the Tat peptide, which also binds with greater affinity to HS than to anionic lipid vesicles (*38*, *51*).

Further thermodynamic characterization of the interaction of R_9 with lipid membranes was achieved by treating the data with a surface partition equilibrium model. More realistic than the previous one, this model considers that R_9 partitions into the membrane from its surface, without assuming a specific interaction between the peptide and lipids. It takes into consideration the electrostatic accumulation of R_9 at the surface of the anionic lipid membrane, and the partition coefficient is calculated with the enhanced surface concentration. For POPC/POPG (75:25) membranes at 28 °C, the partition coefficient was found to be $K = 900$ M^{-1}.

Related studies have been performed for shorter polyarginines measuring the change in the ζ potential of phosphatidylserine vesicles. The measured or extrapolated concentrations of R_5, R_3, and R_2 required to reverse the charge of a PS vesicle were 2×10^{-4}, 3×10^{-3}, and 3×10^{-2} M (*70*). If the ζ potential is reduced to zero, the concentrations of the polycation in the diffuse double layer and in bulk solution are approximately equal and the partition coefficient is given as the inverse of the corresponding concentration, i.e., $K = 5000$ M^{-1} (330 and 33 M^{-1}) for R_5 (R_3 and R_2). Increasing the chain length of the R_n cation hence increases the association constant. The results obtained with ζ-potential measurements refer to pure PS vesicles and are thus not directly comparable to the measurements presented here. However, the same authors have shown for polylysine and mixed PC/PS and PC/PG vesicles that a reduction in the surface charge reduces the association constants by up to 2 orders of magnitude.

Knowledge of the intrinsic partition constant and the R_9 surface concentration allows a discrimination between the electrostatic and nonelectrostatic components of the reaction. Such an analysis is readily made using the following relationship:

$$\Delta G^\circ_{pep,T} = -RT \ln K_P - RT \ln([P]_s/[P]) \qquad (4)$$

where $\Delta G^\circ_{pep,T}$ represents the total free energy of binding, $-RT \ln K_P$ is the nonelectrostatic (hydrophobic and/or hydrogen-bonding) component of $\Delta G^\circ_{pep,T}$, and $-RT \ln([P]_s/[P])$ is the electrostatic component of $\Delta G^\circ_{pep,T}$. On the basis of the data shown in Table 1, we find that $\Delta G^\circ_{pep,T} = -6.1 \pm 0.05$ kcal/mol, which can be divided into an electrostatic binding affinity of -2.1 ± 0.09 kcal/mol and a nonelectrostatic component of -4.1 ± 0.05 kcal/mol. Calculated for a 1 μM bulk concentration of R_9, these values show that only ~33% of the total binding free energy has an electrostatic origin. This contrasts with the data published earlier for the Tat peptide, where ~77% of the free energy of binding is attributed to electrostatics (*51*). Two possible reasons may explain such difference. First, R_9 is inherently more hydrophobic than the Tat peptide. This is explained by the greater hydrophobicity of arginine than lysine, and it is a consequence of the higher arginine content of R_9 when compared to Tat (9 versus 6 arginines). Second, it may also reflect the already mentioned special hydrogen-bond properties of the guanidinium group, which will contribute to a greater nonelectrostatic free energy of binding by interacting with the membrane hydration layer (*vide infra*).

In addition to the partition constant, K_P, the surface partition equilibrium model estimates the effective charge of the peptide, z_P. As shown in Table 1, a $z_P \approx +4$ is found for R_9; this value is smaller than the formal charge of +9 calculated based on the number of charged residues in the peptide. Different effective and formal charges have also been reported for other CPPs (*51*, *71*), demonstrating that not all of the charges in these peptides are available for binding. It reflects the polyelectrolyte behavior of R_9, because

the closely spaced arginines in the peptide attract counterions to its vicinity (counterion condensation), which may not be fully released if the alternative ions bind with moderate or relatively weak affinity. In addition, the high curvature of the sonicated vesicles may prevent a simultaneous approach of all arginines to the membrane surface (*51*).

Even though R_9 binds tightly to anionic lipid vesicles, the deuterium NMR data show no change of the POPC and POPG headgroup conformation when R_9 is added to POPC/POPG (65:35) membranes (parts B and C of Figure 3). This is quite a surprising result, because it is well-known that charged molecules shift the P^--N^+ dipole of the phosphocholine headgroup away or toward the aqueous phase, depending on whether they are negatively or positively charged (*72*). Documented for a large number of chemically distinct compounds, this effect is easily revealed in ^{2}H NMR spectra by a change in the quadrupole splittings of the specifically deuterated phospholipid headgroups (*73*−*75*). Until now, only two exceptions to this general rule have been reported, one being pentalysine (*76*) and the other being the Tat peptide (*51*). In both cases and similarly to what we show here for R_9, the cationic peptides bind to the lipid membrane but binding is not accompanied by a reorientation of phosphocholine headgroup (*51*, *76*). This suggests that these polycationic molecules interact differently with the lipid membrane than, for example, amphipathic peptides such as melittin (*74*, *77*) and that the charged guanidinium residues cannot interact with the phosphocholine dipole. As an alternative mechanism, we therefore suggest hydrogen bonding of R_9 and its analogues to the hydration layer around the lipid headgroup. This hydration layer has an extension of about 1−3 nm, and detailed analysis of the related hydration forces with osmotic experiments has been given by Parsegian and co-workers (*78*). The hydration layer is also reflected in the rate of motion of the phospholipid headgroups, which is almost a factor of 100 times slower than the motion of the free headgroup molecules in bulk water (*79*). To reconcile the strong binding of R_9 to the lipid membrane deduced from ITC with the unchanged headgroup conformation, we suggest that R_9 cannot penetrate between the lipid headgroups but binds at some distance from the headgroups to the hydration layer.

Further structural information regarding the R_9−lipid membrane equilibrium was obtained using phosphorus-31 NMR. This technique is highly sensitive to lipid polymorphism, leading to quite different spectra depending on whether lipid bilayers, hexagonal phases, or micellar phases are present (*55*). The phosphorus NMR spectum shown in Figure 3A is typical of a homogeneous lipid bilayer, providing clear evidence that the POPC/POPG (65:35) membrane is not disrupted upon R_9 binding. Also reported for the Tat peptide (*51*), this observation does not corroborate the formation of nonbilayer structures such as inverted micelles, observed for selected lipids in the case of penetratin (*34*).

HS is a regulatory polysaccharide, which, under *in vivo* conditions, is bound to a variety of integral membrane proteins (*80*). A logical step would therefore be to test R_9 binding to an integral HSPG. Unfortunately, no well-defined model system suited for physical−chemical measurements is known. As an alternative, we have investigated the binding of R_9 to live mouse fibroblasts using the cytosensor microphysiometer. We have applied this method previously to study the metabolic influence of the TAT−PTD peptide and observed a concentration-dependent inhibition of the cellular metabolic activity (*68*). Analogous experiments with R_9 reveal a similar activity of this peptide on the extracellular acidification rate. Control experiments to prove the specificity of R_9 binding to HS on the membrane surface are in progress.

Conclusions. R_9 is the chemically simplest and, at the same time, one of the most efficient CPPs. Two different mechanisms have been investigated for the translocation of CPPs across the cell membrane, namely, (i) the binding of the cationic CPPs to negatively charged lipids, inducing the disruption of the membrane integrity by formation of nonbilayer structures and (ii) the complex formation of CPPs with HS.

The ITC experiments reveal a strong binding of R_9 to anionic lipid vesicles, while, on the other hand, the deuterium and phosphorus NMR studies demonstrate that the bilayer remains intact. In agreement with earlier results obtained with the TAT protein transduction domain (*38*, *51*), it can be concluded that a passive diffusion of CPPs through the lipid bilayer is highly improbable.

Binding of R_9 to HS is characterized by a binding constant that is 2 orders of magnitude larger than that associated with the binding to POPG. Complex formation is driven by electrostatics, and the HS employed in this study can bind up to 7 molecules of R_9. Consequently, the microscopic binding constants for the individual R_9 will vary for statistical reasons with the degree of saturation i according to $K_i = \{K(n + 1 - i)\}/i$. Hence, the ratio between the first and last binding constant will be $\{K_1\}/\{K_n\} = n^2$. However, R_9 will bind sequentially only at very low HS concentrations. At high HS concentrations, as probably encountered on the cell-membrane surface, R_9 can cross link several HS molecules inducing capping phenomena or protein clustering. R_9 binding on the cell surface is also not limited to HS but may occur also with other glycosaminoglycans. Because of the high affinity of R_9 for HS, this could constitute the first step in an endocytic or related pathway of R_9 translocation.

ACKNOWLEDGMENT

We are grateful to Xiaochun Li Blatter for assistance with the ζ-potential measurements. We thank Thomas Anderson for helpful comments on this manuscript.

REFERENCES

1. Lundberg, P., and Langel, U. (2003) A brief introduction to cell-penetrating peptides, *J. Mol. Recognit. 16*, 227−233.
2. Jarver, P., and Langel, U. (2004) The use of cell-penetrating peptides as a tool for gene regulation, *Drug Discovery Today 9*, 395−402.
3. Zhao, M., and Weissleder, R. (2004) Intracellular cargo delivery using tat peptide and derivatives, *Med. Res. Rev. 24*, 1−12.
4. Fawell, S., Seery, J., Daikh, Y., Moore, C., Chen, L., Pepinsky, B., and Barsoum, J. (1994) Tat-mediated delivery of heterologous proteins into cells, *Proc. Natl. Acad. Sci. U.S.A. 91*, 664−668.
5. Schwarze, S. R., Ho, A., Vocero-Akbani, A., and Dowdy, S. F. (1999) *In vivo* protein transduction: Delivery of a biologically active protein into the mouse, *Science 285*, 1569−1572.
6. Astriab-Fisher, A., Sergueev, D., Fisher, M., Shaw, B. R., and Juliano, R. L. (2002) Conjugates of antisense oligonucleotides with the Tat and antennapedia cell-penetrating peptides: Effects on cellular uptake, binding to target sequences, and biologic actions, *Pharm. Res. 19*, 744−754.

7. Torchilin, V. P., Levchenko, T. S., Rammohan, R., Volodina, N., Papahadjopoulos-Sternberg, B., and D'Souza, G. G. M. (2003) Cell transfection *in vitro* and *in vivo* with nontoxic TAT peptide−liposome−DNA complexes, *Proc. Natl. Acad. Sci. U.S.A. 100*, 1972−1977.
8. Nori, A., Jensen, K. D., Tijerina, M., Kopeckova, P., and Kopecek, J. (2003) Tat-conjugated synthetic macromolecules facilitate cytoplasmic drug delivery to human ovarian carcinoma cells, *Bioconjugate Chem. 14*, 44−50.
9. Vives, E., Brodin, P., and Lebleu, B. (1997) A truncated HIV-1 Tat protein basic domain rapidly translocates through the plasma membrane and accumulates in the cell nucleus, *J. Biol. Chem. 272*, 16010−16017.
10. Derossi, D., Joliot, A., Chassaing, G., and Prochiantz, A. (1994) The third helix of the Antennapedia homeodomain translocates through biological membranes, *J. Biol. Chem. 269*, 10444−10450.
11. Wender, P. A., Mitchell, D. J., Pattabiraman, K., Pelkey, E. T., Steinman, L., and Rothbard, J. B. (2000) The design, synthesis, and evaluation of molecules that enable or enhance cellular uptake: Peptoid molecular transporters, *Proc. Natl. Acad. Sci. U.S.A. 97*, 13003−13008.
12. Mitchell, D. J., Kim, D. T., Steinman, L., Fathman, C. G., and Rothbard, J. B. (2000) Polyarginine enters cells more efficiently than other polycationic homopolymers, *J. Pept. Res. 56*, 318−325.
13. Futaki, S., Suzuki, T., Ohashi, W., Yagami, T., Tanaka, S., Ueda, K., and Sugiura, Y. (2001) Arginine-rich peptides. An abundant source of membrane-permeable peptides having potential as carriers for intracellular protein delivery, *J. Biol. Chem. 276*, 5836−5840.
14. Wender, P. A., Rothbard, J. B., Jessop, T. C., Kreider, E. L., and Wylie, B. L. (2002) Oligocarbamate molecular transporters: Design, synthesis, and biological evaluation of a new class of transporters for drug delivery, *J. Am. Chem. Soc. 124*, 13382−13383.
15. Futaki, S., Nakase, I., Suzuki, T., Youjun, Z., and Sugiura, Y. (2002) Translocation of branched-chain arginine peptides through cell membranes: Flexibility in the spatial disposition of positive charges in membrane-permeable peptides, *Biochemistry 41*, 7925−7930.
16. Suzuki, T., Futaki, S., Niwa, M., Tanaka, S., Ueda, K., and Sugiura, Y. (2002) Possible existence of common internalization mechanisms among arginine-rich peptides, *J. Biol. Chem. 277*, 2437−2443.
17. Lundberg, M., and Johansson, M. (2002) Positively charged DNA-binding proteins cause apparent cell membrane translocation, *Biochem. Biophys. Res. Commun. 291*, 367−371.
18. Richard, J. P., Melikov, K., Vives, E., Ramos, C., Verbeure, B., Gait, M. J., Chernomordik, L. V., and Lebleu, B. (2003) Cell-penetrating peptides. A reevaluation of the mechanism of cellular uptake, *J. Biol. Chem. 278*, 585−590.
19. Drin, G., Cottin, S., Blanc, E., Rees, A. R., and Temsamani, J. (2003) Studies on the internalization mechanism of cationic cell-penetrating peptides, *J. Biol. Chem. 278*, 31192−31201.
20. Console, S., Marty, C., Garcia-Echeverria, C., Schwendener, R., and Ballmer-Hofer, K. (2003) Antennapedia and HIV transactivator of transcription (TAT) "Protein transduction domains" promote endocytosis of high molecular weight cargo upon binding to cell surface glycosaminoglycans, *J. Biol. Chem. 278*, 35109−35114.
21. Fittipaldi, A., Ferrari, A., Zoppe, M., Arcangeli, C., Pellegrini, V., Beltram, F., and Giacca, M. (2003) Cell membrane lipid rafts mediate caveolar endocytosis of HIV-1 Tat fusion proteins, *J. Biol. Chem. 278*, 34141−34149.
22. Fuchs, S. M., and Raines, R. T. (2004) Pathway for polyarginine entry into mammalian cells, *Biochemistry 43*, 2438−2444.
23. Fischer, R., Kohler, K., Fotin-Mleczek, M., and Brock, R. (2004) A stepwise dissection of the intracellular fate of cationic cell-penetrating peptides, *J. Biol. Chem. 279*, 12625−12635.
24. Thoren, P. E., Persson, D., Isakson, P., Goksor, M., Onfelt, A., and Norden, B. (2003) Uptake of analogs of penetratin, Tat(48−60) and oligoarginine in live cells, *Biochem. Biophys. Res. Commun. 307*, 100−107.
25. Brugidou, J., Legrand, C., Mery, J., and Rabie, A. (1995) The retro-inverso form of a homeobox-derived short peptide is rapidly internalised by cultured neurones: A new basis for an efficient intracellular delivery system, *Biochem. Biophys. Res. Commun. 214*, 685−693.
26. Derossi, D., Calvet, S., Trembleau, A., Brunissen, A., Chassaing, G., and Prochiantz, A. (1996) Cell internalization of the third helix of the Antennapedia homeodomain is receptor-independent, *J. Biol. Chem. 271*, 18188−18193.
27. Shieh, M., WuDunn, D., Montgomery, R., Esko, J., and Spear, P. (1992) Cell surface receptors for herpes simplex virus are heparan sulfate proteoglycans, *J. Cell Biol. 116*, 1273−1281.
28. Love, D., Esko, J., and Mosser, D. (1993) A heparin-binding activity on Leishmania amastigotes which mediates adhesion to cellular proteoglycans, *J. Cell Biol. 123*, 759−766.
29. Dehio, C., Freissler, E., Lanz, C., Gomez-Duarte, O. G., David, G., and Meyer, T. F. (1998) Ligation of cell surface heparan sulfate proteoglycans by antibody-coated beads stimulates phagocytic uptake into epithelial cells: A model for cellular invasion by *Neisseria gonorrhoeae*, *Exp. Cell Res. 242*, 528−539.
30. Rusnati, M., Coltrini, D., Oreste, P., Zoppetti, G., Albini, A., Noonan, D., d'Adda di Fagagna, F., Giacca, M., and Presta, M. (1997) Interaction of HIV-1 Tat protein with heparin. Role of the backbone structure, sulfation, and size, *J. Biol. Chem. 272*, 11313−11320.
31. Tyagi, M., Rusnati, M., Presta, M., and Giacca, M. (2001) Internalization of HIV-1 Tat requires cell surface heparan sulfate proteoglycans, *J. Biol. Chem. 276*, 3254−3261.
32. Silhol, M., Tyagi, M., Giacca, M., Lebleu, B., and Vives, E. (2002) Different mechanisms for cellular internalization of the HIV-1 Tat-derived cell penetrating peptide and recombinant proteins fused to Tat, *Eur. J. Biochem. 269*, 494−501.
33. Violini, S., Sharma, V., Prior, J. L., Dyszlewski, M., and Piwnica-Worms, D. (2002) Evidence for a plasma membrane-mediated permeability barrier to Tat basic domain in well-differentiated epithelial cells: Lack of correlation with heparan sulfate, *Biochemistry 41*, 12652−12661.
34. Berlose, J. P., Convert, O., Derossi, D., Brunissen, A., and Chassaing, G. (1996) Conformational and associative behaviours of the third helix of antennapedia homeodomain in membrane-mimetic environments, *Eur. J. Biochem. 242*, 372−386.
35. Xu, Y., and Szoka, F. C., Jr. (1996) Mechanism of DNA release from cationic liposome/DNA complexes used in cell transfection, *Biochemistry 35*, 5616−5623.
36. Deshayes, S., Heitz, A., Morris, M. C., Charnet, P., Divita, G., and Heitz, F. (2004) Insight into the mechanism of internalization of the cell-penetrating carrier peptide Pep-1 through conformational analysis, *Biochemistry 43*, 1449−1457.
37. Atherton, E., and Sheppard, R. C. (1989) *Solid-Phase Peptide Synthesis: A Practical Approach*, IRL Press, Oxford, U.K.
38. Ziegler, A., and Seelig, J. (2004) Interaction of the protein transduction domain of HIV-1 TAT with heparan sulfate: Binding mechanism and thermodynamic parameters, *Biophys. J. 86*, 254−263.
39. Hunter, R. J. (1981) *ζ Potential in Colloid Science. Principles and Applications*, Academic Press, London, U.K.
40. Seelig, J. (1997) Titration calorimetry of lipid−peptide interactions, *Biochim. Biophys. Acta 1331*, 103−116.
41. Wieprecht, T., and Seelig, J. (2002) in *Current Topics in Membranes*, pp 31−56, Elsevier Science, New York.
42. Cantor, C. R., and Shimmel, P. R. (1980) in *The Behavior of Biological Macromolecules*, pp 849−885, W. H. Freeman and Company, San Francisco, CA.
43. van Holde, K. E., Johnson, W. C., and Ho, P. S. (1998) in *Principles of Physical Biochemistry*, pp 587−637, Upper Sadle River, NJ.
44. Connors, K. A. (1987) *Binding Constants*, Wiley-Interscience, New York.
45. Mason, J. T., and Huang, C. (1978) Hydrodynamic analysis of egg phosphatidylcholine vesicles, *Ann. N.Y. Acad. Sci. 308*, 29−49.
46. Wiseman, T., Williston, S., Brandts, J. F., and Lin, L. N. (1989) Rapid measurement of binding constants and heats of binding using a new titration calorimeter, *Anal. Biochem. 179*, 131−137.
47. Seelig, J., Nebel, S., Ganz, P., and Bruns, C. (1993) Electrostatic and nonpolar peptide−membrane interactions. Lipid binding and functional properties of somatostatin analogues of charge $z = +1$ to $z = +3$, *Biochemistry 32*, 9714−9721.
48. Terzi, E., Holzemann, G., and Seelig, J. (1994) Alzheimer β-amyloid peptide 25−35: Electrostatic interactions with phospholipid membranes, *Biochemistry 33*, 7434−7441.
49. Terzi, E., Holzemann, G., and Seelig, J. (1995) Self-association of β-amyloid peptide (1−40) in solution and binding to lipid membranes, *J. Mol. Biol. 252*, 633−642.

50. Wenk, M. R., and Seelig, J. (1998) Magainin 2 amide interaction with lipid membranes: Calorimetric detection of peptide binding and pore formation, *Biochemistry 37*, 3909−3916.
51. Ziegler, A., Blatter, X. L., Seelig, A., and Seelig, J. (2003) Protein transduction domains of HIV-1 and SIV TAT interact with charged lipid vesicles. Binding mechanism and thermodynamic analysis, *Biochemistry 42*, 9185−9194.
52. Hiemenz, P. C., and Rajagopalan, R. (1997) *Principles of Colloid and Surface Chemistry*, 3rd ed., Marcel Dekker, Inc., New York.
53. Nebel, S., Ganz, P., and Seelig, J. (1997) Heat changes in lipid membranes under sudden osmotic stress, *Biochemistry 36*, 2853−2859.
54. Beschiaschvili, G., and Seelig, J. (1990) Peptide binding to lipid bilayers. Binding isotherms and ζ-potential of a cyclic somatostatin analogue, *Biochemistry 29*, 10995−11000.
55. Seelig, J. (1978) ^{31}P nuclear magnetic resonance and the head group structure of phospholipids in membranes, *Biochim. Biophys. Acta 515*, 105−140.
56. Wohlgemuth, R., Waespe-Sarcevic, N., and Seelig, J. (1980) Bilayers of phosphatidylglycerol. A deuterium and phosphorus nuclear magnetic resonance study of the head group region, *Biochemistry 19*, 3315−3321.
57. Seelig, A., Allegrini, P. R., and Seelig, J. (1988) Partitioning of local anesthetics into membranes: Surface charge effects monitored by the phospholipid head group, *Biochim. Biophys. Acta 939*, 267−276.
58. Lewis, G. N., Randall, M., Pitzer, K. S., and Brewer, L. (1961) *Thermodynamics*, 2nd ed., McGraw−Hill, New York.
59. Murphy, K. P., and Gill, S. J. (1991) Solid model compounds and the thermodynamics of protein unfolding, *J. Mol. Biol. 222*, 699−709.
60. Gelman, R. A., Glaser, D. N., and Blackwell, J. (1973) Interaction between chondroitin-6-sulfate and poly-L-arginine in aqueous solution, *Biopolymers 12*, 1223−1232.
61. Gelman, R. A., and Blackwell, J. (1973) Interactions between mucopolysaccharides and cationic polypeptides in aqueous solution: Chondroitin 4-sulfate and dermatan sulfate, *Biopolymers 12*, 1959−1974.
62. Gelman, R. A., and Blackwell, J. (1974) Interactions between mucopolysaccharides and cationic polypeptides in aqueous solution: Hyaluronic acid, heparitin sulfate, and keratan sulfate, *Biopolymers 13*, 139−156.
63. Hileman, R. E., Jennings, R. N., and Linhardt, R. J. (1998) Thermodynamic analysis of the heparin interaction with a basic cyclic peptide using isothermal titration calorimetry, *Biochemistry 37*, 15231−15237.
64. Fromm, J. R., Hileman, R. E., Caldwell, E. E. O., Weiler, J. M., and Linhardt, R. J. (1997) Pattern and spacing of basic amino acids in heparin binding sites, *Arch. Biochem. Biophys. 343*, 92−100.
65. Griffin, C. C., Linhardt, R. J., van Gorp, C. L., Toida, T., Hileman, R. E., Schubert, I., Robert L., and Brown, S. E. (1995) Isolation and characterization of heparan sulfate from crude porcine intestinal mucosal peptidoglycan heparin, *Carbohydr. Res. 276*, 183−197.
66. Sakai, N., and Matile, S. (2003) Anion-mediated transfer of polyarginine across liquid and bilayer membranes, *J. Am. Chem. Soc. 125*, 14348−14356.
67. Record, M. T., Jr., Anderson, C. F., and Lohman, T. M. (1978) Thermodynamic analysis of ion effects on the binding and conformational equilibria of proteins and nucleic acids: The roles of ion association or release, screening, and ion effects on water activity, *Q. Rev. Biophys. 11*, 103−178.
68. Ziegler, A., Nervi, P., Dürrenberger, M., and Seelig, J. (2004) The cationic cell-penetrating peptide CPPTAT derived from the HIV-1 protein TAT is rapidly transported into living fibroblasts: Optical, biophysical, and metabolic evidences, *Biochemistry*, in press.
69. Rothbard, J. B., Jessop, T. C., Lewis, R. S., Murray, B. A., and Wender, P. A. (2004) Role of membrane potential and hydrogen bonding in the mechanism of translocation of guanidinium-rich peptides into cells, *J. Am. Chem. Soc. 126*, 9506−9507.
70. Kim, J., Mosior, M., Chung, L. A., Wu, H., and McLaughlin, S. (1991) Binding of peptides with basic residues to membranes containing acidic phospholipids, *Biophys. J. 60*, 135−148.
71. Thoren, P. E., Persson, D., Esbjorner, E. K., Goksor, M., Lincoln, P., and Norden, B. (2004) Membrane binding and translocation of cell-penetrating peptides, *Biochemistry 43*, 3471−3489.
72. Seelig, J., Macdonald, P. M., and Scherer, P. G. (1987) Phospholipid head groups as sensors of electric charge in membranes, *Biochemistry 26*, 7535−7541.
73. Akutsu, H., and Seelig, J. (1981) Interaction of metal ions with phosphatidylcholine bilayer membranes, *Biochemistry 20*, 7366−7373.
74. Kuchinka, E., and Seelig, J. (1989) Interaction of melittin with phosphatidylcholine membranes. Binding isotherm and lipid head group conformation, *Biochemistry 28*, 4216−4221.
75. Beschiaschvili, G., and Seelig, J. (1991) Peptide binding to lipid membranes. Spectroscopic studies on the insertion of a cyclic somatostatin analog into phospholipid bilayers, *Biochim. Biophys. Acta 1061*, 78−84.
76. Roux, M., Neumann, J. M., Bloom, M., and Devaux, P. F. (1988) ^{2}H and ^{31}P NMR study of pentalysine interaction with headgroup deuterated phosphatidylcholine and phosphatidylserine, *Eur. Biophys. J. 16*, 267−273.
77. Beschiaschvili, G., and Seelig, J. (1990) Melittin binding to mixed phosphatidylglycerol/phosphatidylcholine membranes, *Biochemistry 29*, 52−58.
78. Rand, R. P., and Parsegian, V. A. (1989) Hydration forces between phospholipid bilayers, *Biochim. Biophys. Acta 988*, 351−376.
79. Scherer, P. G., and Seelig, J. (1987) Structure and dynamics of the phosphatidylcholine and the phosphatidylethanolamine head group in L−M fibroblasts as studied by deuterium nuclear magnetic resonance, *EMBO J. 6*, 2915−2922.
80. David, G. (1993) Integral membrane heparan sulfate proteoglycans, *FASEB J. 7*, 1023−1030.

BI048046I